Thickness- and Deposition Rate-Dependence of Structural Characteristics of Evaporated CdTe Films

M. R. Ebeid[1], M. F. Ahmed[1], A. A. Ramadan[2] and K. Abdel-Hady[1]

[1] Physics Department, Minia University, Minia, EGYPT
[2] Physics Department, Helwan University, Helwan, Cairo, EGYPT

The dependence of the structural characteristics of evaporated CdTe films on the deposition parameters was investigated by X-ray diffraction. All deposited films were single phase of cubic zincblende structure and showed strong preferential orientation with <111> fiber texture. The Voigt method of single reflection was used for line profile analysis to determine the crystallite size and microstrain. The internal microstrain decreases sharply at smaller thickness and became thickness-independent for values larger than 500 nm, where as the degree of preferred orientation and the crystallite size increase monotonously. The increase of deposition rate was found to improve the stoichiometry, to increase the degree of preferred orientation and to decrease the crystallite size as well as the internal microstrain. The structural characteristic variations were discussed in relation to the effect of the deposition parameters during film preparation.

1. Introduction:

Cadmium telluride (CdTe) is very interesting semiconductor in the form of thin films; it is one of the most promising polycrystalline materials for producing opto-electronic devices [1] and photovoltaic cells [2]. Thus, this material has been grown by a wide variety of techniques and recently by pulsed laser deposition [3 - 5] and stacked elemental layer processing [6]. The structure of CdTe films is sensitive to preparation conditions and exists into two different types (cubic zincblende and hexagonal wurtzite structure). Spinulescu-Carnaru [7] has reported that films with pure wurtzite structure are obtained by deposition on heated substrate when Te and metallic Cd are co-evaporated in an Ar atmosphere. When thin films of CdTe were deposited on mica by vacuum condensation in a quasi- closed cell, Yezhovsky and Kalinkin [8] found that large source-substrate temperature differences promoted wurtzite growth, where as under conditions close to equilibrium only cubic growth occurred. Films prepared by RF sputtering [9] showed hexagonal

wurtzite structure which was found to be independent of the preparation conditions except the substrate bias voltage. It was also found that the film structure depends on the substrate orientation [10 - 12].

The structure of evaporated CdTe films was of the cubic zincblende type with a preferential orientation of the (111) plane parallel to the substrate [13 - 16]. On contrast, films prepared by pulsed laser deposition [5], using low energy, showed a preferental orientation of the (220) plane. However, their depicted diffraction patterns is not a good one, and the broad (111) and sharp (220) reflections in the same diffractogram (Fig.1a in ref. [5]) is a question mark. Saha *et al.* [15] observed a gradual increase in the crystallite size and gradual decrease in the internal strain and dislocation density as well as the stacking fault probability up to a thickness of 700 nm beyond which the values of the crystallite size decreased. Ismail and Gould [16] evaporated CdTe films with thickness up to 1 μm and observed that they are microcrystalline with grain size of 74 nm.

Thus, the both the structure and orientation of evaporated CdTe films are greatly influenced by the preparation parameters. However, poor quantitative determination of the structural parameters has been reported. So, the objective of this work is to study extensively the effect of the thickness and deposition rate on structure characteristics preferential orientation, crystallite size and microstrain of thermally evaporated CdTe thin films.

2. Experimental and Calculations:

Films were prepared from the high purity CdTe powder (99.999%) by the physical thermal evaporation onto glass substrates kept at 20 cm from the material boat. The glass substrates were cleaned ultrasonically and washed with alcohol, dried and rubbed gently with cotton. Final cleaning was achieved by ionic bombardment inside the vacuum chamber during the first stage of evacuation by using the high-voltage source for a period of about 10 min. The substrate-temperature was kept at fixed temperature of 150°C. This specific substrate temperature is the minimum one that avoid the condensation of free tellurium [17]. The vacuum during evaporation process was kept at 1.3×10^{-4} Pa. The evaporation rate and film thickness were controlled by a quartz crystal monitor which was pre-calibrated by an interferometric method. For investigating the effect of film thickness, films were prepared at fixed rate of evaporation (0.5 nm/s) while the thickness was varied within the range 126 to 1115 nm. The effect of the deposition rate was investigated in a range from 0.5 to 2.5 nm/s while the film thickness was kept constant at 470 ± 5 nm.

Jeol X-ray diffractometer (model JSDX-60 PA) was used with Ni filtered Cu $K\alpha$ radiation at 50 kV and 15 mA. The intensity data were collected using the step-scanning mode with a small step size ($\Delta 2\theta = 0.05^{\circ}$). A period of 10 s at each step of 2θ was found enough to yield a reasonable number of counts at each peak maximum. Also, a standard KCl sample was investigated under the same conditions used for prepared films in order to determine the instrumental broadening. Rietveld refinement algorithm [18] was applied to the diffraction pattern of CdTe powder in order to verify the presence of a single phase and to specify accurately its characterization. This was achieved using a computer program written by Lutterotti *et al.* [19] with graphical presentation. Figure (1) shows the final refinement, illustrating the difference between the experimental and calculated data (lower part in the diagram) in addition to vertical lines in the top of the graph at the position of the possible Bragg reflections of CdTe phase corresponding to the given model. The obtained Reliability factor and the Goodness-of-fit are R_{wp} = 11.53 % and S = 2.78, respectively.

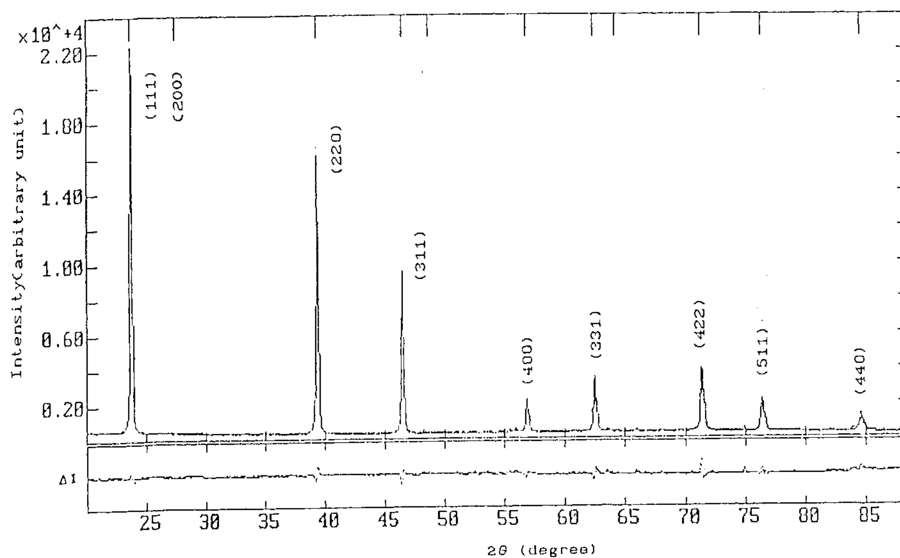

Fig. (1) : Rietveld refinement of the diffracted patterns of CdTe powder. (R_{wp}= 11.53 % and Goodness-of-fit, S = 2.78)

There is more than one method for single reflection line profile analysis. However, the Voigt analysis [20] is the one of the most considerable interest for its ability to (i) allow for separation of instrumental and specimen contribution and (ii) model size- and strain- line broadening contribution

simultaneously. The Voigt function is the analytical convolution product of a Lorentzian (Cauchy, C) function to model the contribution of the size broadening, and Gaussian (G) function to model those of the strain. If the line profile is assumed to be Voigtian, then

$$h_C(2\theta)*h_G(2\theta) = f_C(2\theta)*f_G(2\theta)*g_C(2\theta)*g_G(2\theta) \quad (1)$$

where h, f and g are the observed-, specimen- and instrumental-profile functions, respectively.

A parameter of interest with the Voigt function is "the shape parameter", ϕ, defined as the ratio of the full-width at half maximum(FWHM) to the integral breadth (IB), thus, ϕ = FWHM / IB. The value of this parameter is used to determine the fractional Lorentzian and Gaussian components in the convolute. Asthana and Kiefer [21] gave a simple expression to determine the Lorentzian (β_C) and Gaussian (β_G) components of the observed and instrumental profiles from the observed and standard diffraction data as following:

$$\beta C/\beta = 2.0207 - 0.4803\,\phi - 1.7756\,\phi 2 \quad (2)$$

and

$$\beta_G/\beta = 0.6420 + 1.4187(\phi - 2/\pi)^{1/2} - 2.202043\,\phi + 1.8706\,\phi^2 \quad (3)$$

Then, the Lorentzian and Gaussian components of the integral breadth of the corrected profile(f) representing the specimen characteristics are given by

$$\beta_{fC} = \beta_{hC} - \beta_{gC} \quad (4)$$

and

$$\beta^2_{fG} = \beta^2_{hG} - \beta^2_{gG} \quad (5)$$

Accordingly, Sherrer equation is used to model the broadening due to the crystallite size, L,

$$L = \lambda/(\beta_{fC}\cos\theta) \quad (6)$$

and the strain broadening is constrained according to

$$e = \beta_{fG}/(4\tan\theta) \quad (7)$$

3. Results and Discussion:

3.1. Film thickness-dependence

The diffraction patterns for films of different thicknesses (Fig. (2)) indicating the presence of only a single phase of CdTe, which is of the cubic zincblende structure. Since the substrate temperature and deposition rate are kept constant, no variation in the film stoichiometry is expected. Therefore, the observed overall increase of intensity is essentially due to the increase in the material volume scattering X-rays. However, in all cases the relative intensity of the (111) diffraction peak was very high compared with the randomly-oriented powder. This confirms the preferential orientation of the (111) plane parallel the substrate, i.e., <111> fiber-like texture. The variation of the degree of such preferred orientation was found to increase with the film thickness as proved by the variation of the intensity ratio $[I_{(111)}/I_{(220)}]$ illustrated in Fig.(3a). Thus, as the film grows, the effect of the disorder structure of the amorphous (glass) substrate is gradually masked and the degree of preferred orientation (ordering) ascends.

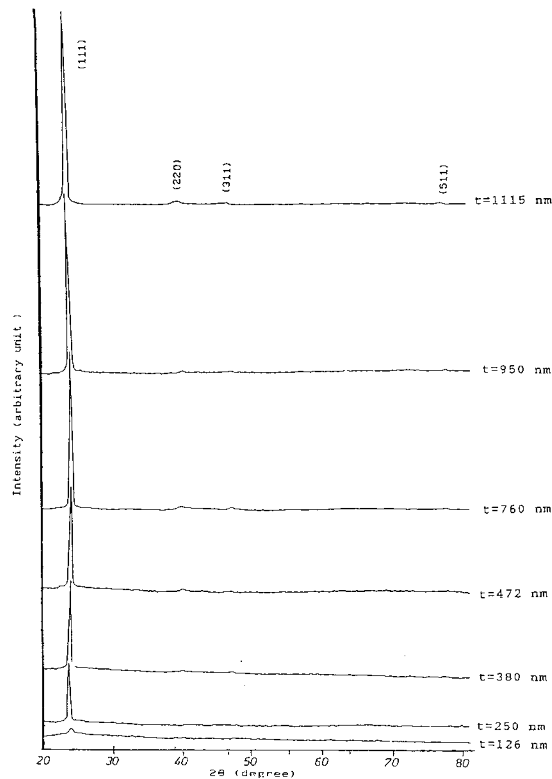

Fig. (2) : X-ray diffractograms of films with different thicknesses.

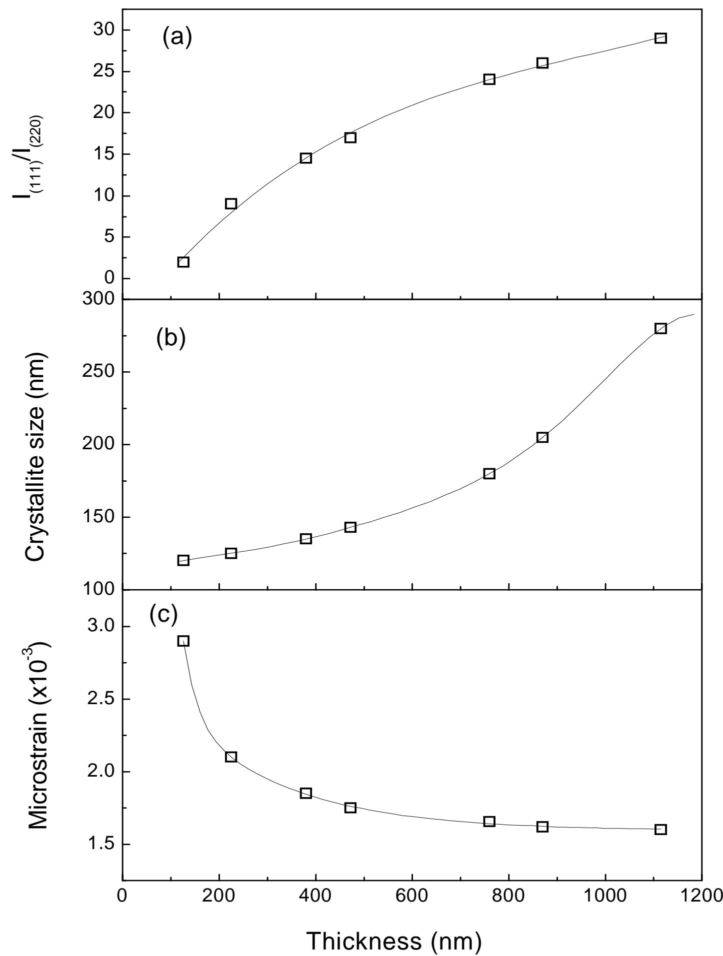

Fig.(3): Effect of film thickness on: (a) degree of preferred orientation ($I_{(111)}/I_{(220)}$), (b) crystallite size and (c) microstrain. (r = 0.5 nm/s, T_s=150 ^oC)

FWHM was found to decrease markedly with increasing film thickness for thinner films and then gradually at higher thickness. Such decrease reflects the decrease in the contribution of the internal microstrain within the films due to lattice imperfections, such as structural defects and non-stoichiometry, and/or an increase in the crystallite size. This was confirmed quantitatively by line profile analysis. Due to the high degree of preferred orientation only one order of reflection can be measured accurately enough and then the Voigt single order analysis was applied. From experimentally observed and instrumental standard diffraction data, crystallite size, L, and microstrain, e, were calculated using Eqns. (2-7).

Figure (3b) shows the crystallite size calculated from the (111) reflection as a function of the film thickness. A considerable increase of the crystallite size was observed with a probable upper limit of about 300 nm for films thicker than 1200 nm. The crystallite size is, by definition, measured in direction normal to the reflection plane, i.e., in the <111> direction, consequently perpendicular to the substrate. Therefore, the observed increase in the crystallite size may be interpreted in terms of a columnar grain growth. On the other hand, the microstrain exhibited a contrast behaviour, i.e., decreases sharply at small thickness and going to be thickness-independent for thick films, as indicated in Fig.(3c). This variation may be due to the increase of ordering (degree of preferred orientation) and the decrease of the structural defects among which the grain boundary. Saha *et al*. [15] observed the same behaviour but the increase and decrease in the size and strain, respectively, take place gradually.

3.2. Deposition rate-dependence

In order to study the effect of deposition rate, the film thickness was kept constant at 470±5 nm. This value was considered since the crystallite size and microstrain were slightly varied within this range of thickness as shown in Fig.(3). The X-ray diffractograms (Fig.(4)) show that all CdTe films, within the large range of deposition rate applied in the present work, exhibit high degree of the <111> fibre-like texture. Figure (5a) shows the variation of the intensity ratio $I_{(111)}/I_{(220)}$, indicating that the degree of preferred orientation increases with increase of the deposition rate. The variation is very small in comparison to that due to the effect of film thickness (Fig. (3a)). Such increase seems to be a result of the high energy of the impinging atoms at higher rates. The energy increases the mobility of the atoms on the substrate to a sufficient value to aggregate themselves in the closed packing form [22]. This enables the atoms to orient themselves to form the optimum orientation growth. In case of the cubic zincblende structure, it is the (111) plane that one of the atomic density. it is worthy to mention that, with increasing the deposition rate, not only the relative intensity of the (111) reflection increases but also the absolute value. This observed increase could be discussed in relation to the change in the structure factor.

The integrated intensity of certain Bragg reflection is proportional to the structure factor, F, [23]. If the identity of an atom is changed or a new one is added, and it does not cause a change in the crystal structure, modified structure factor will be obtained [24]. Thus, the effect of randomly located point defects on the observed intensities requires modification of the atomic scattering factor. The effective scattering term, f^{eff}, is an average of the

constituent atoms occupying that site where a vacancy is represented by scattering factor f_V =0.0 [25]. In this fashion, the atomic scattering factor of the Cd should be "modified" by the presence of vacancies (V_{Cd}) and that of Te by the presence of vacancies (V_{Te}) or antisites (Cd_{Te}), i.e. Cd in the Te-site. The effective atomic scattering factors [26] are then given as:

$$f_{Cd}^{eff} = (1-x)f_{Cd} + x\, f_V, \quad (9)$$

and

$$f_{Te}^{eff} = (1-(y+z))f_{Te} + y\, f_V + z\, f_{Cd} \quad (10)$$

Since the atomic scattering factor of Te is greater than that of Cd, the increase in the absolute values of the measured intensities seems to be a result of the increase of the "effective" scattering factor of f_{Cd} and/or f_{Te}, due to the decrease in the concentration of vacancies (V_{Cd} or V_{Te}) and/or antisites (Cd_{Te}). This expected decrease in the density of lattice defects (vacancies and antisites) based on the experimental results of the intensity, is also in agreement with the decrease of the measured microstrain at higher growth rates. Voigt profile analysis (Eqns.(2-7)) was also used to study quantitatively the small variation of the FWHM resulting from varying the deposition rate. Fig (5b) indicates a decrease in the crystallite size with the deposition rate. This is because at higher rates of film formation more nuclei are initially formed, from which a fine grain grows. Also, increasing the deposition rate was found to cause a decrease of the microstrain as indicated in Fig.(5c). The short time allowed for deposition at higher rates lead to lower concentration of contamination. This may also interpret the observed decrease in the interplanar spacing which was calculated from position of (111) reflection. The interplanar spacing decreases gradually (from 0.3754 to 0.3753 nm) as the deposition rate increases. Since the contaminations (e.g. O_2, N_2.... etc.) are in general of smaller atomic size compared with both Cd and Te, they interstice between the atoms in the original lattice. Thus, the decrease in their concentration results in shorter interplanar spacing. The two types of bonding should be also considered, as the ionic radii of Te^{-2} and Cd^{+2} are 0.221 and 0.097 nm and their tetrahedral covalent radii are 0.132 and 0.148 nm, respectively. Therefore, the decrease in d-spacing as the Te/Cd ratio increases (decreases of Cd_{Te} antisites) may indicate the increasing contribution of the covalent-type [27] as the density of lattice defect decreases.

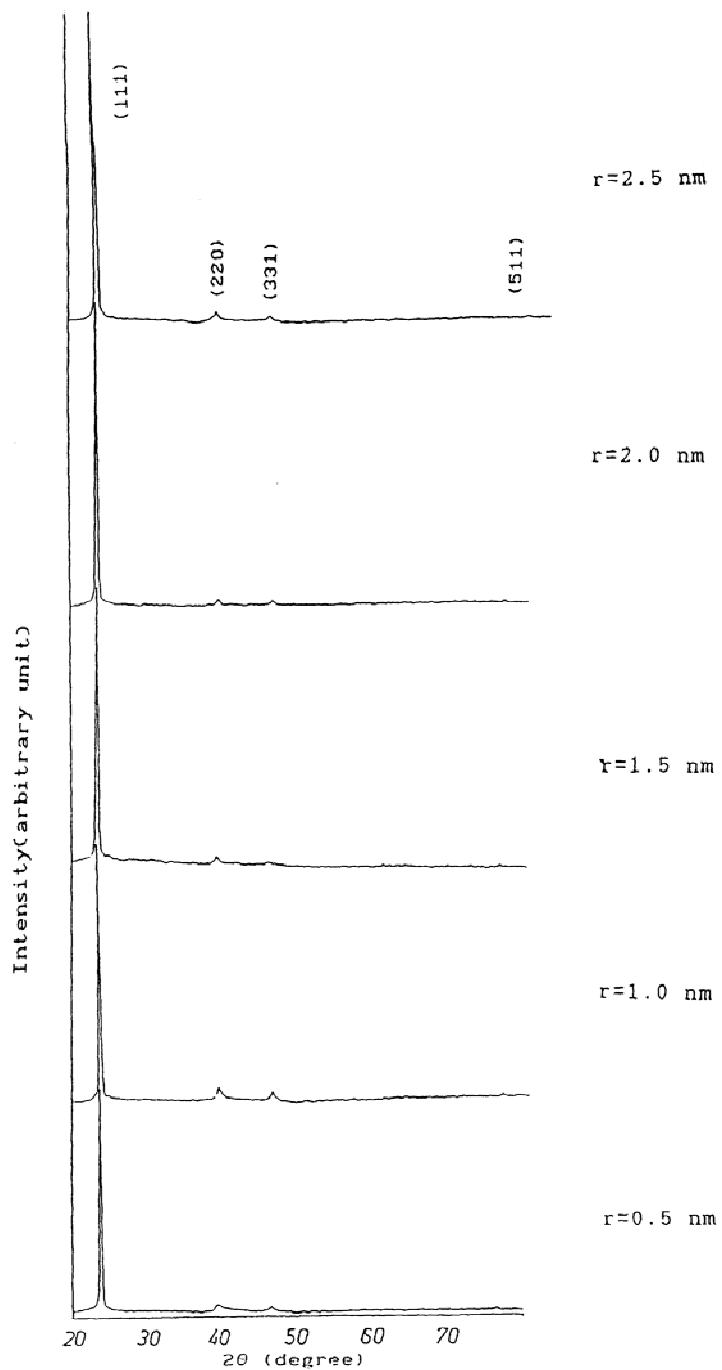

Fig. (4) : X-ray diffractograms of films with different deposition rates.
(t = 470 nm, T_s=150 ^oC)

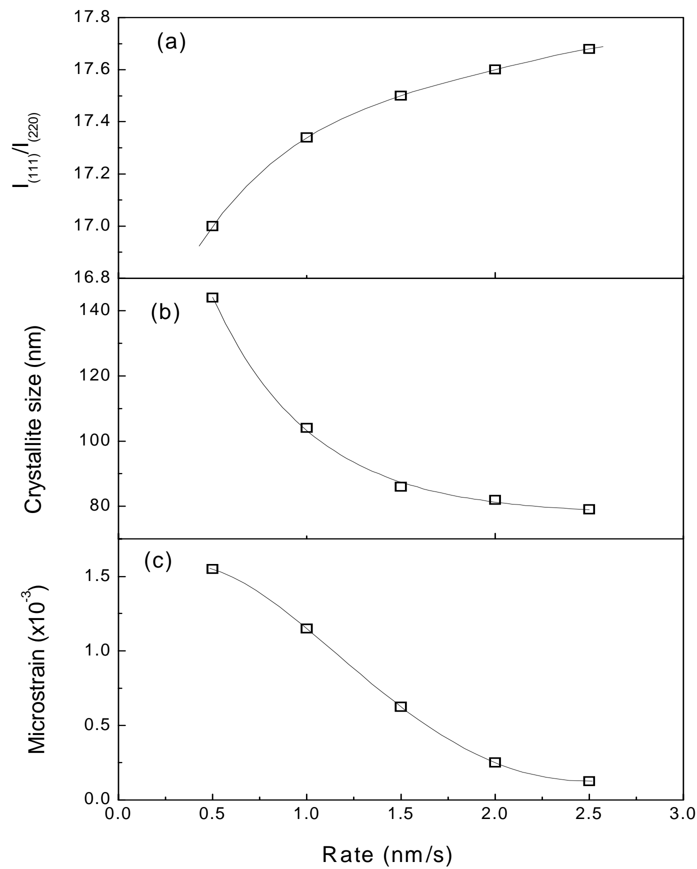

Fig. (5): Effect of deposition rate on: (a) degree of preferred orientation ($I_{(111)}/I_{(220)}$), (b) crystallite size and (c) microstrain. (t = 470 nm, T_s=150 ^oC)

4. Conclusions:

All deposited films showed a strong <111> fibre-like texture and the degree of preferred orientation increases as the film thickness or deposition rate increases. With increasing the film thickness, microstrain was observed to decrease sharply at smaller thickness whereas the crystallite size increases. On the other hand, both the microstrain and crystallite size decrease as the deposition rate ascends. For thick films (>500 nm), the microstrain becomes thickness-independent and at high rates (>1.5 nm/s), both the crystallite size and microstrain become rate-independent. The increase in the diffraction intensity as the deposition rate increases is assumed to be due to the decrease in the concentration of vacancies (V_{Cd} or V_{Te}) and/or antisites (Cd_{Te}). Also, the contribution of the covalent bonding may increase as the structural defects decrease.

References:

1. M. B. Das, S. V. Krishnaswamy, R. Petkie, P. Swab, K. Vams, *Solid State Electron* **27,** 329 (1984).
2. E. Rakhashani, *J. Appl. Phys*. **81,** 7988 (1997).
3. F. Jackson, L. E. A. Berlousis, P. Rocabois, B. C. Cavenett, *J. Crystal Growth* **159,** 200 (1996).
4. A. Giardini, M. Ambrico, D. Smaldne, R. Martino, G. P. Parisi, V. Capozzi, G. Perna, *Appl. Surf. Sci*. **106,** 144 (1996).
5. Ramiro, J., Perea, A. Trigo, J. F. Laaziz, Y., Camarero, E.G.: *Thin Solid Films* **361-362,** 65 (2000).
6. Cruz, L. R., Kazmerski, L. L., Moutinho, H. R., Hasoon, F., Dhere, R. G., De Avillez, R.: *Thin Solid Films* **350,** 44 (1999).
7. Spinulescu Curnaru, I.:*phys. stat. sol*. **15 ,** 761 (1966).
8. Yezhovsky, Y. K., Kalinkin, I. P.: *Thin solid Films* **18,** 12 (1973).
9. De Laplaza, M., Gonzalez-Diaz, G., Sachez-Quesada, F., Rodriguez-Vidal, M.: *Thin Solid Films* **120,** 31 (1984).
10. Holt, D. B., Abdalla, M.: *phys. stat. sol*. (a) **26,** 507 (1974).
11. Holt, D. B., *phys. stat. sol. (a)* **29,** 29 (1975).
12. Holt, D. B., *Thin solid Films* **37,** 91 (1976).
13. Kawai, Y, Ema, Y., Hayashi, T.: *Thin Solid Films* **147**, 75 (1987).
14. Hayashi, T, Suzuki, T., Ema, Y.: *Jap. J. Appl. Phys*. **27,** 1626 (1988).
15. Saha, S., Pal., U., Samantaray B. K., Chaudhuri. A. K.: *Thin Solid Films* **164,** 85 (1988).
16. Ismail, B. B., Gould, R. D.: *phys. stat. sol. (a)* **115,** 327 (1989).
17. Glang, R., Kren, J. G., Patrick, W. J.: *J. Electrochem. Soc*. **110,** 407 (1963).
18. [18] McCusker, L. B., Von Dreele, R. B., Cox, D. E., Louer, D., Scardi, P.: *J. Appl. Cryst.* **32,** 36 (1999).
19. Lutterotti, L., Scardi, P., Maistrelli, P.: *J. Appl. Cryst*. **25,** 459 (1992).
20. Langford, J. I., Loüer, D.: *Rep. Prog. Phys*. **59,** 131 (1996).
21. Asthana, B. P., Kiefer, W.: *Appl. Spectrosc*. **36,** 250 (1982).
22. Post, J. E., Bish, D.L.: “*Modern Powder Diffraction*” Mineralogical Society of America, Reviews in Mineralogy, **20,** 276 (1989).
23. Glusker, J. P., Lewis, M., Rossi, M.: "*Crystal Structure Analysis for Chemists and Biologists*", VCH Pub., Inc., New York, p.15. (1994).
24. Glusker, J. P.; "*Crystallography: Teaching and Applications*", Proc. Egyptian 5th Int. Sch. of Cryst., Edt: K. El-Sayed and A. A. Ramadan, Suez, Egypt. April, p.18 (1997).
25. Albin, D., Noufi, H., Tuttle, J., Risbud, S. H.: *J. Appl. Phys*. **64,** 4903 (1988).
26. Aibinati, A., Willis, B. T. M.: *J. Appl. Cryst*. **15,** 361 (1982).
27. De Noble, D.: *Philips Res. Rep*. **14,** 361 (1959).